REPORT DOCUMENTATION PAGE

Form Approved
OMB No. 0704-0188

1. REPORT DATE *(DD-MM-YYYY)*	2. REPORT TYPE	3. DATES COVERED *(From - To)*
09-02-2005	REPRINT	

4. TITLE AND SUBTITLE
Ion-molecule kinetics at 15-700 Torr

5a. CONTRACT NUMBER

5b. GRANT NUMBER

5c. PROGRAM ELEMENT NUMBER
61102F

6. AUTHOR(S)
A. A. Viggiano, Abel I. Fernandez, and J. Troe*

5d. PROJECT NUMBER
2303

5e. TASK NUMBER
BM

5f. WORK UNIT NUMBER
A1

7. PERFORMING ORGANIZATION NAME(S) AND ADDRESS(ES)
Air Force Research Laboratory/VSBXT
29 Randolph Road
Hanscom AFB, MA 01731-3010

8. PERFORMING ORGANIZATION REPORT NUMBER
AFRL-VS-HA-TR-2005-1038

9. SPONSORING/MONITORING AGENCY NAME(S) AND ADDRESS(ES)

10. SPONSOR/MONITOR'S ACRONYM(S)

11. SPONSOR/MONITOR'S REPORT NUMBER(S)

12. DISTRIBUTION/AVAILABILITY STATEMENT
Approved for public release; distribution unlimited.

13. SUPPLEMENTARY NOTES
REPRINTED FROM: Physical Chemistry Chemical Physics, Vol. 7, 2005, pp1533-1539
*Institut fur Physikalische Chemie, Universitat Gottingen, Tammannstrasse 6, D-37077, Gottingen, Germany.

14. ABSTRACT

Studies of ion–molecule chemistry are usually made at pressures of a few Torr and below. By contrast, there are numerous plasmas that occur at higher pressures. For that reason we have constructed a turbulent ion flow tube (TIFT) for studying ion–molecule kinetics from 15 to 700 Torr. Currently, the TIFT operates from room temperature to 700 K. Here we present a summary of the measurements we have made to date. The first measurements involved SF_6^- reactions with SO_2, H_2O, CH_3OH and C_2H_5OH at room temperature. The SO_2 reaction showed the same kinetics as low pressure measurements indicating that the reaction occurs rapidly. The other reactions were all found to be cluster-mediated with branching fractions that depend on pressure. More recently, charge transfer reactions of O_2^+ to alkylbenzenes have been studied at elevated temperatures, from 400 to 700 K. Both dissociative and non-dissociative charge transfer occurs with the latter being favored at high pressures indicating that excited states live long enough to be stabilized by the buffer gas. Combining the TIFT measurements with detailed statistical adiabatic channel model/classical trajectory (SACM/CT) calculations of the unimolecular decay constant allows energy transfer parameters to be derived. Extending the temperature range upwards to 750 K has allowed thermal decomposition rate constants to be measured. The thermal decomposition has been successfully modeled using the same parameters as for the collision quenching modeling. This allows bond strengths for the dissociation to be derived with high accuracy. Both the measurements and models show that the conditions correspond to the high pressure kinetics regime.

15. SUBJECT TERMS
High pressure kinetics
Dissociation rate constants

16. SECURITY CLASSIFICATION OF:			17. LIMITATION OF ABSTRACT	18. NUMBER OF PAGES	19a. NAME OF RESPONSIBLE PERSON
a. REPORT	b. ABSTRACT	c. THIS PAGE			A. A. Viggiano
UNCL	UNCL	UNCL	UNL		19b. TELEPHONE NUMBER *(Include area code)* (781) 377-4028

RESEARCH PAPER

PCCP
www.rsc.org/pccp

Ion–molecule kinetics at 15–700 Torr†

A. A. Viggiano,[a] Abel I. Fernandez‡[a] and J. Troe*[b]

[a] *Air Force Research Laboratory, Space Vehicles Directorate, 29 Randolph Rd., Hanscom Air Force Base, MA 01731-3010, USA*
[b] *Institut für Physikalische Chemie, Universität Göttingen, Tammannstrasse 6, D-37077 Göttingen, Germany. E-mail: shoff@gwdg.de*

Received 16th November 2004, Accepted 24th January 2005
First published as an Advance Article on the web 9th February 2005

Studies of ion–molecule chemistry are usually made at pressures of a few Torr and below. By contrast, there are numerous plasmas that occur at higher pressures. For that reason we have constructed a turbulent ion flow tube (TIFT) for studying ion–molecule kinetics from 15 to 700 Torr. Currently, the TIFT operates from room temperature to 700 K. Here we present a summary of the measurements we have made to date. The first measurements involved SF_6^- reactions with SO_2, H_2O, CH_3OH and C_2H_5OH at room temperature. The SO_2 reaction showed the same kinetics as low pressure measurements indicating that the reaction occurs rapidly. The other reactions were all found to be cluster-mediated with branching fractions that depend on pressure. More recently, charge transfer reactions of O_2^+ to alkylbenzenes have been studied at elevated temperatures, from 400 to 700 K. Both dissociative and non-dissociative charge transfer occurs with the latter being favored at high pressures indicating that excited states live long enough to be stabilized by the buffer gas. Combining the TIFT measurements with detailed statistical adiabatic channel model/classical trajectory (SACM/CT) calculations of the unimolecular decay constant allows energy transfer parameters to be derived. Extending the temperature range upwards to 750 K has allowed thermal decomposition rate constants to be measured. The thermal decomposition has been successfully modeled using the same parameters as for the collision quenching modeling. This allows bond strengths for the dissociation to be derived with high accuracy. Both the measurements and models show that the conditions correspond to the high pressure kinetics regime.

Introduction

High pressure ion–molecule reactivity studies have traditionally been limited to less than 5 Torr. Only occasionally have studies been made above this range. In 1996, Knighton and Grimsrud[1] summarized all studies in what they termed the "very high pressure" (VHP) regime, *i.e.* from 0.01 to 10 atm. At that time, they found less than 20 VHP papers and few more have been published since. The need for such data is obvious since many plasmas occur at or near atmospheric pressure. Examples include the Earth's atmosphere,[2,3] plasma assisted combustion,[4] and plasmas around fast moving vehicles in the lower atmosphere.[5,6] In addition, a number of analytical instruments involve VHP plasmas including atmospheric pressure mass spectrometers, ion mobility spectrometers, and electron capture detectors in gas chromatographs.

It is well known that pressure can quench certain species and affect the yield of products. For this to occur, the time between collisions of the buffer gas and the intermediate species must be less than or on the order of the lifetime of the intermediate state. At atmospheric pressure, typical collision times are on the order of 10^{-10} s. Since ion–molecule reactions often involve long lived complexes, many reactions may have intermediates that live long enough to encounter a collision with the buffer gas.

Several techniques have been used to make measurements in the VHP regime. These have been summarized in the review of Grimsrud and Knighton.[1] They pointed out that flow tubes had never been used for such studies but that they should be an excellent platform for such studies. Seeley *et al.*[7] developed a turbulent ion flow tube for neutral studies. Since ions are lost on every collision with walls, and this instrument had minimal wall losses, the adaptation to ion studies seemed straightforward and practical. With all the above in mind, our group at the Air Force Research Laboratory (AFRL) developed such an instrument. So far, studies have been made from 15–700 Torr and from 300–700 K. This paper reviews the development of the instrument and all the studies performed to date.

Experimental

The AFRL turbulent ion flow tube (TIFT) is based on the instrument designed by Seeley *et al.* for neutral kinetics.[7] The current version of the instrument is shown in Fig. 1. The instrument has gone through moderate changes since the first version,[8] mainly to introduce temperature variability. In many ways, the TIFT operates similarly to low pressure flow tubes used for ion–molecule reaction studies[9] and indeed the same software controls both the low and high pressure apparatuses in our laboratory.[10,11] In all ion flow tubes, ions are created, carried down an approximately one metre tube by a large carrier gas flow, and sampled into a mass spectrometer. Neutral reagents are added at various intermediary points. The main difference between the low and high pressure instruments is that the TIFT uses larger buffer gas flow rates which results in turbulent instead of laminar flow. Turbulent flow is obtained for Reynolds numbers greater than 3000.[12]

The buffer enters the flow tube through a sidearm as shown in Fig. 1. Typical flow rates are 40–80 standard litre per minute (slm), which makes N_2 taken from liquid as the most practical and economic choice. Note that a 1A cylinder of gas lasts only about an hour and needs to be trapped to rid the gas of impurities. While this is possible, it is expensive and requires

† Presented at the Bunsen Discussion on Chemical Processes of Ions, Marburg, 15–17 September 2004.
‡ Abel I. Fernandez, is a National Academy of Sciences Postdoctoral Fellow.

DOI: 10.1039/b417454b

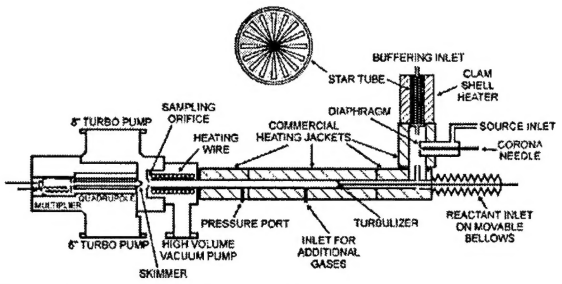

Fig. 1 Schematic view of the variable temperature turbulent ion flow tube (TIFT).

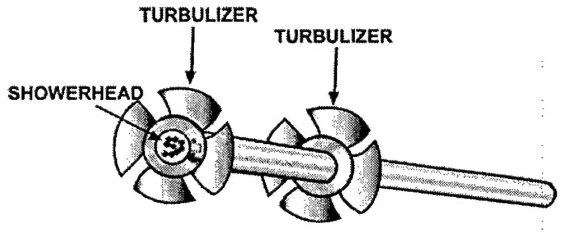

Fig. 2 Schematic of the neutral injector design with turbulizers attached.

much attention. The large flow rate requires the gas to be preheated since wall collisions in the flow tube are not sufficient for the gas to come into equilibrium with the wall temperature.[13] The current design has the gas flowing through a stainless steel rod with star shaped flow channels being cut into it as shown in the insert in Fig. 1. The tube is heated by cylindrical clamshell heaters. The temperature of the gas exiting the heater is regulated to the flow tube temperature as measured by a thermocouple at the end of the reactant inlet. It is necessary to overheat the gas by about 100 °C to compensate for heat losses in the upstream end of the apparatus and for introduction of unheated source gas.

A corona discharge ion source (coaxial cylinder geometry) creates ions in the sidearm. The corona is separated from the main flow by a cup with a 1 mm exit hole. This allows the corona to run at relatively high pressure even when the flow tube is operated at 15 Torr. The corona so far has been used to make only O_2^+. The first experiments used pure O_2 in the corona, although it was recently found that a mixture of mainly Ar ($\approx$1 slm) with a small amount of O_2 ($\approx$3 standard cubic centimetres per minute, sccm) yields a stronger ion signal at low pressure. The Ar/O_2 combination also greatly reduces the amount of $[O_2]$ needed ($\approx$1% of the pure O_2 case) which reduces interference from neutral O_2 in the study of some slow reactions. Higher Ar flows are found to be necessary at high pressure to prevent backstreaming. In order to reduce water, the corona gases are passed through a molecular sieve trap at approximately −100 °C (methanol slush bath). The voltage on the corona varies with condition from 1000–5000 V, typically 2000 V. The position of corona needle can be adjusted and the tip is typically less than 1 cm upstream of the orifice. The cup periodically needs to be sanded to rid it of an unwanted oxidation layer which causes ion signal degradation. The sidearm, except for the corona holder, is heated to the flow tube temperature by a heating jacket. The first studies involving SF_6^- used a Po-210 radioactive ion source instead of the corona at room temperature only. Experiments at elevated temperatures require preheating of the gas (see above) but because the Po foil would melt, it was necessary to switch to the corona source. Other sources have not been explored at this time.

The heated gas enters the flow tube and is carried past a neutral injector where the reactant neutral is added. Rate constants and branching ratios are typically measured by fixing the distance and varying the reagent flow rate. A flush gas coflows with the reagent to reduce the effective volume of the injector. This proved important for operation at pressures approaching 100 Torr and above to reduce settling time. The injector distance can be changed and the kinetic measurements repeated. This allows mixing times to be estimated. With a truncated straight tube as the inlet, exceedingly long mixing times were found. To circumvent this, two fan blades and a showerhead were added to create small local eddies which promote turbulent flow and enhance mixing. The injector with these additions is shown in Fig. 2. The additions greatly reduced the mixing time. The turbulizers and showerhead were added one at a time and all three were needed to reduce the effective mixing distance to less than approximately one cm. A thin thermocouple is placed at the end of the moveable tube to measure the gas temperature.

The flow tube is heated in four zones. The three outside the sampling region are broken up into two relatively short end zones and a long central one. All use jacket heaters with built in thermocouples. Additional inlets are incorporated for adding gases or measuring the ion velocity. The pressure is controlled by a MKS control valve. The inside zone is heated by ceramic coated wire.

The gas is sampled through a truncated nose cone with a 50–150 micron orifice. The ensuing supersonic beam is skimmed and sampled into a quadrupole mass spectrometer. The ions are detected by a discrete dynode particle detector. Both the nose cone and skimmer are isolated and voltages are applied.

In order to measure accurate rate constants, the ion velocity must be known since it is well known that ion velocities are greater than the bulk flow velocity.[9] In laminar flow the profile of the neutral velocities is parabolic, with the centerline velocity being twice the average. The ion profile is peaked on the central axis since at the boundary ions are lost to the walls with almost complete efficiency. When ions are sampled from the center, the average velocity is typically around to 1.6 times the average due to diffusion. In turbulent flow, the neutral velocity profile is closer to being square shaped and the centerline velocity is much closer to the average velocity. In order to accurately account for this, it is best to measure the ion velocity. We have done this in the TIFT by pulsing thin wires at two distances from the nose cone and looking for the time at which the ion disturbance reached the detector. The ratio of ion velocity to buffer velocity was found to vary from $\approx$2 for the peak neutral velocity at low Reynolds numbers to $\approx$1 at very high Reynolds numbers.[8] Under typical operating conditions, the ratio is about 1.1 to 1.2. No dependence on pressure was found.

By measuring the ion velocity, the mixing distance, as well as all the normal flow tube parameters such as pressure, temperature and flow rates, the error for this instrument is believed to be similar to that for other fast flow apparatuses. The error limits are quoted as ±15% relative error and ±25% absolute error. At present we have made measurements from 15–700 Torr. Below about 25 Torr, it is not possible to run in the turbulent flow regime since the pump is not fast enough. Rate constants are more difficult to measure at the low pressures but branching ratios are not as problematic since they rely only on the relative signals of two or more ions. At present we have made measurements from 300 to 700 K and have plans to increase this upper temperature limit by 100–200 K.

Frequently, impurities have been a problem, particularly water vapor. This requires baking of the instrument and inlet lines as well as trapping of the corona gases and He when it has been used as a buffer. This has limited operation to ions that do not react with H_2O or an oxygen impurity in the N_2 buffer. At room temperature, SF_6^- was made quite cleanly. Above 423 K, O_2^+ can be made cleanly. Below this temperature, oxygen

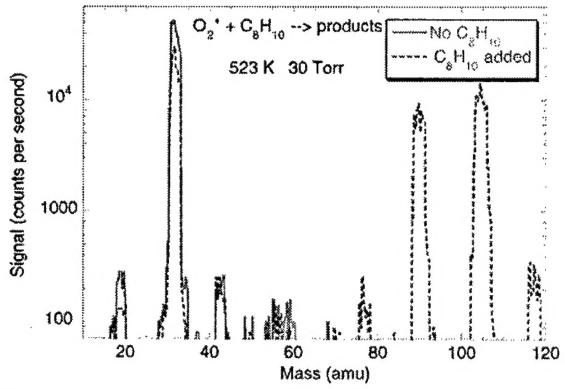

Fig. 3 Low-resolution mass spectra with and without ethylbenzene reagent in the study of O_2^+ with C_8H_{10}.

clusters rapidly to water and then forms $H_3O^+(H_2O)_n$ ions.[14] These impurities frequently limit the highest pressure at which branching fractions can be measured. When reporting branching ratios, ionic impurities are limited to less than 3%; this is needed to avoid falsification of the branching ratio measurements by parallel/competitive reactions. A typical spectrum with O_2^+ as the primary ion and with and without neutral ethylbenzene reagent gas is shown in Fig. 3. Without reagent, there are less than one percent impurity ions. Presently we can do even better (by reducing small leaks and more baking). The exception is non-reactive alkali ions, *e.g.*, Na^+, K^+, that are emitted from surfaces at high temperatures. Note that the spectra in Fig. 3 were taken under low resolution conditions to minimize mass discrimination since it is not possible to quantify mass discrimination in this instrument. Our experience indicates that the low resolution spectra have little discrimination since ion balance is good. In order to account for ionic species separated by one or two masses, the low resolution spectra are supplemented by higher resolution spectra. For example, in the hydrocarbon work discussed below, ions at both 91 and 92 amu are present. The total intensity of this doublet is recorded with low resolution where the peaks completely overlap and the contribution of each peak is assigned by high resolution spectra. This works well since mass discrimination is rarely important for ions separated by one amu.

During sampling a supersonic expansion is formed. Clustering in the expansion can be a problem. It is difficult to determine whether clustering occurred in the flow tube or in the expansion. In one of our studies (see below) it was clear that some of the clustering did occur in the expansion. In that case, we could tell because the equilibrium constants were known. For other species, this is difficult to determine especially when the temperature is not at 300 K because the area near the nose cone may have a slightly reduced temperature, which of course affects the equilibrium constant. For this reason we have avoided pure clustering studies.

We have also worried about dissociation in the sampling region. If the electric fields are high, dissociation can occur. We check this by varying the electric field and looking for changes in distributions. At the highest voltages we apply, dissociation has been observed. We believe we have eliminated dissociation for the most part by using reduced fields. The one exception is in our original study of SF_6^- with SO_2 where dissociation was calibrated.

Results and discussion

The first study using the TIFT was of the reaction of SF_6^- with SO_2 at 300 K over the pressure range 25–700 Torr.[8] This was mainly a proof-of-principle study for which we did not expect large pressure dependences. The reaction had been studied previously[15,16] and three product ions were known to be formed,

$$\begin{aligned} SF_6^- + SO_2 &\rightarrow SF_5^- + FSO_2 \\ SF_6^- + SO_2 &\rightarrow FSO_2^- + SF_5 \\ SF_6^- + SO_2 &\rightarrow F_2SO_2^- + SF_4. \end{aligned} \quad (1)$$

In this work and in the previous studies only the charged species were observed; thus, the neutral products given above are presumed to exist. Since SF_6^- does not react with any common impurities, both rate constants and products ratios could be studied. Because this reaction is not expected to have a pressure dependence and because the rate constants, 1.0×10^{-9} cm^3 s^{-1} over the entire pressure range, are in good agreement with previous low pressure measurements, these results showed that the TIFT can be used to make accurate kinetic measurements over the wide pressure range. The product distribution was also found to be invariant and consistent with the low pressure measurements. The average values are 24, 60 and 16% for SF_5^-, $F_2SO_2^-$, and FSO_2^-, respectively. The lack of a pressure dependence in either the branching ratio or rate constant indicates that the lifetime of an SF_6^-–SO_2 complex is shorter than the lifetime with respect to collisions with the N_2 buffer gas, which is 70 ps at 700 Torr.

A study of the reactivity of SF_6^- with H_2O, CH_3OH and C_2H_5OH from 50 to 500 Torr at 298 K proved more interesting.[17] The first reaction is important in electrical discharges when SF_6 is used as a high voltage gaseous dielectric. Studies of all three reactions showed the decline of the SF_6^- parent to be second order in the solvent. The mechanism, shown for water vapor, is

$$SF_6^- + H_2O \rightleftarrows SF_6^-(H_2O) \quad (2)$$

$$SF_6^-(H_2O) + H_2O \rightarrow SF_4O^- + 2HF + H_2O \quad (3a)$$

$$SF_6^-(H_2O) + H_2O \rightarrow F^-(HF)_2(H_2O)_{0,1} + [\,SF_3O(H_2O)_{1,0}\,], \quad (3b)$$

In the TIFT, the amount of clustering in the products is controlled by secondary equilibrium and does not represent the nascent distribution. For the alcohols the products are $F^-(HF)$ and $F^-(HF)_2$ solvated to an indeterminable extent.

The slope of the decline in the SF_6^- signal *vs.* solvent squared yielded the product of the equilibrium constant for reaction (2) and the rate constant for reaction (3). The ratio of $[SF_6^-][X]]/[SF_6^-(X)]$ would be expected to yield the equilibrium constant. The ratio was found not to depend on solvent concentration of the solvent X as expected for equilibrium. However, it was found that the ratio was dependent on pressure, which was interpreted to involve clustering in the supersonic expansion. Fortunately, equilibrium constants were available from other measurements and rate constants could be derived. The rate constants for reaction (3) were found to be very small and pressure independent within a larger than normal error (factor of two). For H_2O, CH_3OH, and C_2H_5OH, the rates averaged to be 0.32, 1.9 and 2.2×10^{-13} cm^3 s^{-1}, respectively. These values would be extremely difficult, if not impossible, to measure in a low pressure or non flow apparatus.

The branching ratios depend on pressure. Fig. 4 shows the fraction of the $F^-(HF)_2(ROH)_n$ product *vs.* pressure. As a reminder, the other product is SF_4O^- for H_2O and $F^-(HF)(ROH)_n$ for the alcohols. The branching for the H_2O case is approximately constant. This indicates that the products may separate quickly on the time scale of collisions with N_2. For the alcohols, the $F^-(HF)_2(ROH)_n$ products increase substantially with pressure at the expense of the $F^-(HF)(ROH)_n$ channel. A larger effect is observed for C_2H_5OH. This was speculated to be a result of a two step

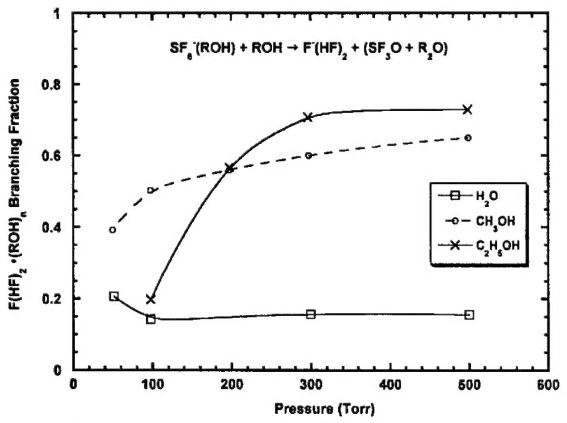

Fig. 4 Branching fraction of the $F^-(HF)_2(ROH)_n$ channel for the reactions of SF_6^- with H_2O, CH_3OH and C_2H_5OH as a function of pressure. (Parentheses indicate that the nature of the neutrals is unknown.)

mechanism where the second step is slow compared to buffer gas collisions. The buffer gas can cool the complex allowing for more time for the second proton transfer to occur. Alternatively, the cooling can prevent HF from evaporating from a hot intermediate. The latter explanation is more in line with our charge transfer work discussed below.

The most recent studies have involved charge transfer from O_2^+ to alkylbenzenes.[18–20] In these experiments, the buffer gas affects the reactivity in two ways. The processes occurring are shown schematically for the ethylbenzene reaction in Fig. 5. Reaction is started by charge transfer, which leaves the $C_8H_{10}^+$ ion in excited states which partially dissociate. The amount of and rate for dissociation depends on the charge transfer mechanism.[21] A direct resonant mechanism leaves essentially all alkylbenzene ions with enough energy to dissociate as indicated by the distribution marked direct; the resonant charge transfer product has an excitation energy of about 4 eV, much greater than thermal. If the reaction proceeds through a complex, the distribution of alkylbenzene ions is much broader and part of the distribution will not have enough energy to dissociate. This is indicated by the fraction α in the diagram. At low pressure, all molecules with energy above the dissociation limit are expected to dissociate unless radiative quenching or wall collisions compete with dissociation.

The dissociation of alkylbenzene ions takes place on the time scale of collisions with the buffer gas.[22–24] Thus, increasing the pressure increases the amount of the nondissociative parent ion observed by cooling the distribution. A collision with a buffer gas molecule removes an average energy per collision $\langle\Delta E\rangle$.[20] Combining TIFT measurements of the branching ratio for stabilized parent to dissociated fragments (S/D) with measurements of the unimolecular rate constants for dissociation as a function of energy allows for a derivation of $\langle\Delta E\rangle$ per collision

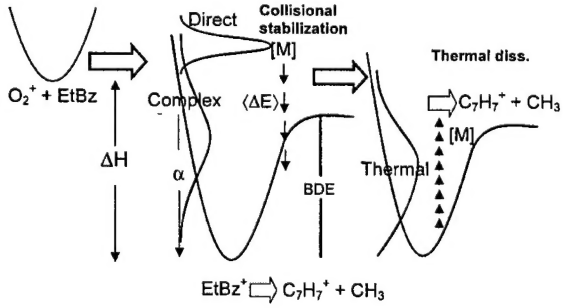

Fig. 5 Schematic view of the processes started by the reaction of O_2^+ with C_8H_{10} (ethylbenzene).

to be made.[20] After numerous collisions, a Boltzmann distribution of energies is found as indicated by the thermal distribution in the far right panel of Fig. 5. At high temperatures, the distribution extends into the range where $C_8H_{10}^+$ can dissociate and thermal dissociation takes place. As will be shown below, both stabilization and dissociation have been observed with both ethylbenzene and propylbenzene.

The first system studied was O_2^+ with C_8H_{10} (ethylbenzene) over the temperature range from 423 to 573K.[19,20] The lower limit was set by the temperature where the water impurity led to an unacceptable amount of non-O_2^+ ions and the upper limit was set partly by experimental constraints (see above) and partly by the desire to avoid thermal dissociation in that study. Current studies have led to an increase of the upper temperature limit so that the thermal dissociation process can be studied. Mostly an N_2 buffer was used but several points were also taken in He. The mechanism depicted in Fig. 5 in the absence of thermal dissociation can be summarized as

$$\begin{aligned}
&O_2^+ + C_8H_{10} \rightarrow C_8H_{10}^+ + O_2 \quad (k = \alpha k_{cap})\\
&O_2^+ + C_8H_{10} \rightarrow (C_8H_{10}^+)^* + O_2 \quad (k = (1-\alpha)k_{cap})\\
&(C_8H_{10}^+)^* + M \rightarrow C_8H_{10}^+ + M \quad (k = \gamma_c Z)\\
&(C_8H_{10}^+)^* \rightarrow C_7H_7^+ + CH_3 \quad (k = k(E)) \qquad (4)
\end{aligned}$$

where k_{cap} is the capture rate constant, γ_c is the stabilization efficiency, Z is the collision rate with respect to the buffer, and $k(E)$ is the dissociation rate as a function of energy. The $C_7H_7^+$ ion has two isomeric forms; benzylium, a six membered ring, and tropylium, a seven membered ring. Most of the product is the former, since it results from a simple benzylic bond cleavage.[25] There are minor products (see Fig. 3) which are no more abundant than the impurity ions and were not followed.

Rate constants were found to be equal to the collisional value and independent of both temperature and pressure. This was expected based on the low pressure results. In contrast, the branching ratios were found to be highly pressure and temperature dependent. Fig. 6 shows the ratio of $C_8H_{10}^+$ to $C_7H_7^+$ as a function of the N_2 buffer gas density. The data clearly show that the buffer gas is quenching the dissociation. Increasing pressure increases the ratio linearly within the scatter in the data. Increasing the temperature results in a shallower slope. The intercepts show no measurable trend. Measurements made using helium buffer at 523 K also yield linear data but with a shallower slope than that found for N_2 at the same temperature. This shows that N_2 is a better quencher than He as expected. Solving the kinetics in reaction (4) yields the

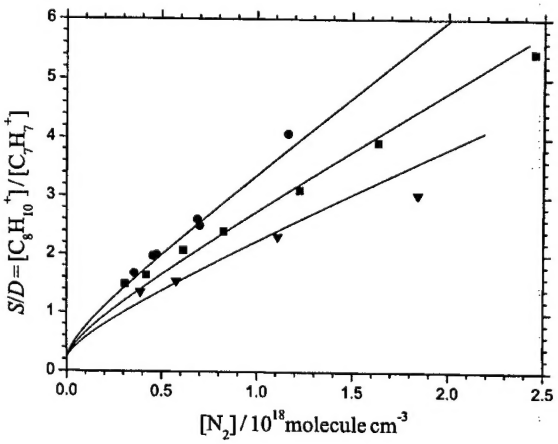

Fig. 6 Ratio of $C_8H_{10}^+$ to $C_7H_7^+$ yield as a function of N_2 number density for the reaction of O_2^+ with C_8H_{10}. The lines are model fits to the data as explained in the text. ●, ■ and ▲ refer to data at 423, 473 and 523 K, respectively.

following expression for the branching ratio (S/D),

$$\frac{[C_8H_{10}^+]}{[C_7H_7^+]} \approx \frac{\alpha}{1-\alpha} + \frac{\gamma_c Z[M]}{(1-\alpha)k(E)} \quad (5)$$

This simple one-state model predicts a linear dependence on $[M]$ in accord with the data within our error.

In this model, the slope of the TIFT data is $\frac{\gamma_c Z}{(1-\alpha)k(E)}$. Therefore, knowledge of $k(E)$ allows γ_c to be derived. Additionally it has been shown that if $k(E) \propto (E - E_0)^{s^*-1}$ then $\langle \Delta E \rangle$ can be derived from

$$\frac{\gamma_c}{1-\gamma_c^n} \approx \frac{-\langle \Delta E \rangle s^*}{E_{ac} - E_0} \quad (6)$$

where E_{ac} is the energy of $C_8H_{10}^{+}$* after charge transfer, n is an exponent close to 2, and E_0 is the bond dissociation energy.[26] $k(E)$ has been measured by two groups but outside our energy range.[23,24] To compensate, statistical adiabatic channel model/classical trajectory (SACM/CT) calculations have been made.[27] The details of the calculations are only summarized here. A model potential is used such that in the reaction coordinate it is a mix of (a) a long-range, charge-induced dipole potential and (b) a short-range valence potential. Anisotropy is also included in the short-range valence potential. Conserved modes are treated by SACM and the bond breaking modes are treated by CT. The absolute magnitude of $k(E)$ is fixed at a single point by adjusting the bond dissociation energy. It is shown that pure statistical calculations are not valid because the Massey parameter indicates that the dynamics are non-adiabatic. The $k(E)$ curves fit the complete experimental data set and are proportional to $(E - E_0)^{s^*-1}$. Thus, eqn. (6) can be used to calculate $\langle \Delta E \rangle$.

While the above discussion gives the underlying theory for such derivations, it is of course better to account for broad energy distributions arising from charge transfer. This has also been done. The first step is to derive the energy distributions in $C_8H_{10}^{+}$* after the charge transfer but before quenching. Three mechanisms are possible, (a) resonant charge transfer, (b) complex formation followed by a statistical dissociation into the products, and (c) production of electronically excited O_2. The first two are depicted in Fig. 5 and the latter contributes only to α. Statistical theory is used to calculate the energy distributions for each mechanism. In order to assign contributions to each of the mechanisms, three data sets were combined. The fraction of non-dissociated $C_8H_{10}^{+}$ in ICR[25] and molecular beam experiments[28] at near zero pressure is assigned as the fraction corresponding to mechanism (c) since the production of excited state O_2 leads exclusively to products that do not dissociate. The TIFT extrapolation to zero pressure does not equal the low pressure values and one Torr measurements are in between the extrapolated TIFT and the low pressure value. These facts indicate that both of the other mechanisms are operative and allow for assignment of the probability of mechanisms (a) and (b). In this way, the assigned probabilities are 0.26, 0.56 and 0.18 for mechanisms (a)–(c), respectively. The data did not warrant a temperature dependence of these fractions but the distributions were allowed to be temperature dependent. The ratio of $C_8H_{10}^{+}$ to $C_7H_7^{+}$ was calculated and shown in Fig. 6 for each temperature. The calculations fit the data very well and show that the data would curve at pressures lower than can be measured in the TIFT. The intermediate pressure range is due to the changing distribution of the complex-forming channel. The pressure range in low pressure flow tubes is not large enough to measure an appreciable dependence accurately.

Finally, it is possible to derive $\langle \Delta E \rangle$, the average energy transferred per collision. Using the best estimates of the various contributions to the mechanism above, $\langle \Delta E \rangle$ is found to be 285 ± 150 cm^{-1} for N_2 and 180 ± 90 cm^{-1} for He at an average energy of 26 600 cm^{-1}. These values are, within uncertainty limits, equivalent to those of neutral toluene at the same energy.[29] Thus, the main difference between energy transfer between ions and neutrals is due to the collision rate and not the amount of energy transferred. Because the energy transfer probably takes place on the repulsive part of the potential, which is likely similar for both ions and neutrals, the equivalence is not surprising. This contrasts to vibrational energy transfer for low lying states.[30] In that state-to-state regime, energy transfer is dominated by complex formation for ions and is much faster than that found for the corresponding neutrals.

The above experiments and calculations were repeated using n-propylbenzene as the reactant neutral.[18] It was possible to extend the conditions of the measurements in two ways. First, the amount of water vapor impurity was reduced by fixing leaks and baking the apparatus; this allowed minor products to be measured accurately. Secondly, the upper temperature limit was increased to allow for thermal decomposition studies. This involved replacing seals and installing the star shaped heat exchanger and clamshell heaters. The minor channels appeared to behave similarly to the main dissociation channel forming $C_7H_7^{+}$, *i.e.* quenching the charge transfer complex affected all channels equally within our uncertainty.

There was enough scatter to prevent detection of small changes.

Adding a thermal dissociation channel,

$$C_9H_{12}^{+} + M \rightarrow C_7H_7^{+} + C_2H_5 + M, \quad (7)$$

creates kinetics that are slightly more complicated. If one assumes that either the excited state charge transfer product dissociates or a Boltzmann distribution of $C_9H_{12}^{+}$ dissociates one derives,

$$\frac{S}{D} \approx \frac{(S/D)_0\,[1 - \exp(-k_{td}t)]}{k_{td}t\,(1 + (S/D)_0) - (S/D)_0[1 - \exp(-k_{td}t)]} \quad (8)$$

where S/D, the stabilization-to-dissociation ratio, is the ratio of $C_9H_{12}^{+}$ to $C_7H_7^{+}$, $(S/D)_0$ is this ratio in the absence of thermal dissociation, and k_{td} is the thermal dissociation rate constant. This expression refers to the zero depletion limit, which is a good assumption since the branching ratio data are obtained by extrapolating to zero concentration of C_9H_{12}. $(S/D)_0$ and k_{td} are obtained separately by studying the kinetics at various reaction times by moving the inlet. Data obtained at 100 Torr and at two temperatures are shown in Fig. 7. The lines are non-linear least squares fits using eqn. (8). The thermal dissociation study was performed at 573 and 603 K as a function of pressure. Table 1 shows the thermal

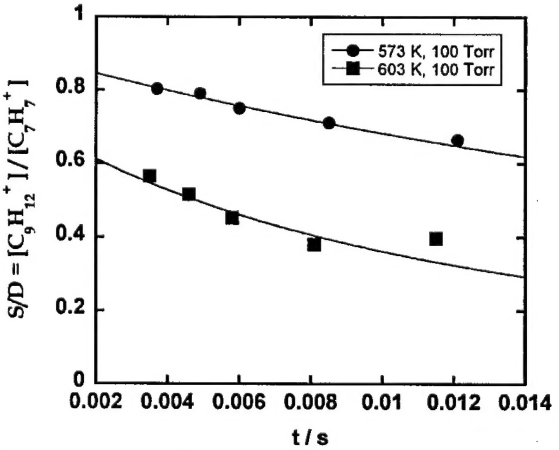

Fig. 7 The ratio of $[C_9H_{12}^{+}]/[C_7H_7^{+}]$ is plotted *vs.* reaction time at pressures of 100 Torr of N_2 for the reaction of O_2^{+} with C_9H_{12}. Fits to eqn. (8) are shown as curves.

Table 1 Thermal dissociate rate constants of $C_9H_{12}^+$ from O_2^+ + C_9H_{12} as a function of temperature and pressure

T/K	P/Torr	k_{td}/s^{-1}
573	50	37
	75	44
	100	32
	150	22
	200	27
	250	34
	30	101
603	50	109
	75	109
	100	98
	150	75
	200	109
	250	138

dissociation rates. The data are somewhat scattered with the 603 K data being less so due to the larger rate constant which suggests that the measurements at 603 K are more reliable. Because the data are independent of pressure with experimental error, this indicates that the system is in the high pressure regime. As explained below, calculations confirm this conclusion.

Fig. 8 shows the S/D data and model fits. Included is $(S/D)_0$ when thermal dissociation plays a role in the kinetics. $C_8H_{10}^+$ and $C_9H_{12}^+$ have nearly equal dissociation energies. Because of the larger number of oscillators, one would expect that $k(E)$, at the same $E - E_0$, is smaller for $C_9H_{12}^+$ than for $C_8H_{10}^+$. However, because the two molecules apparently have different distributions of oscillator frequencies, $k(E)$ is about a factor of two larger for $C_9H_{12}^+$ than the corresponding value for $C_8H_{10}^+$. As a consequence, higher pressures for collisional stabilization are required for $C_9H_{12}^+$ than for $C_8H_{10}^+$.

A derivation that is as detailed as for the ethylbenzene reaction proved difficult for two reasons. Firstly, it was not possible to precisely assign fractions to the various mechanisms. Secondly, the $k(E)$ data are not known as well. In any case, a similar analysis was done and the results are shown in Fig. 8. It is clear that the results do not fit the data as well for reasons that are not obvious although the reasons cited above

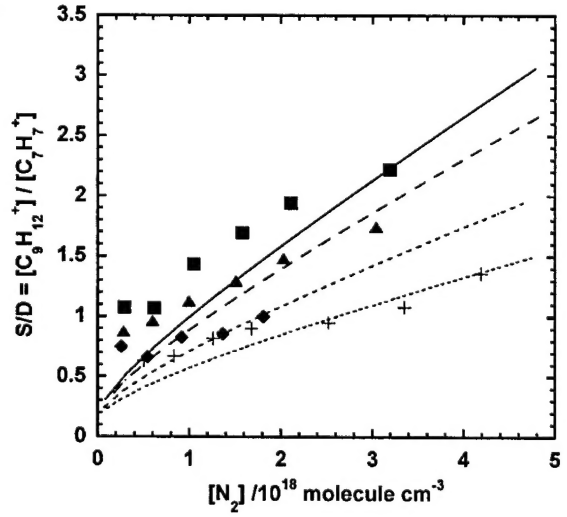

Fig. 8 Ratio of $C_9H_{12}^+$ to $C_7H_7^+$ yields as a function of N_2 number density for the reaction of O_2^+ with C_9H_{12}. The lines are model fits to the data as explained in the text. Squares, triangles, diamonds, and crosses refer to data at 448, 473, 523 and 573 K, respectively.

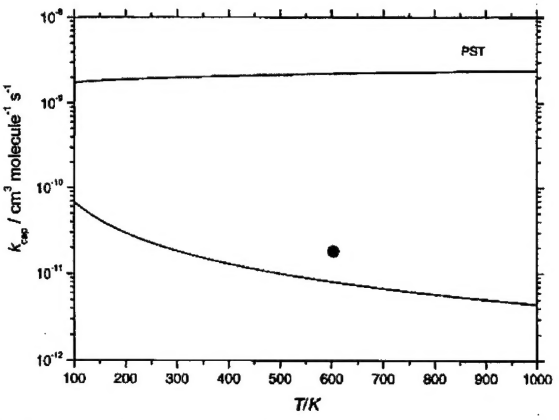

Fig. 9 Recombination rate constants $k_{cap} = k_{rec,00}$ for $C_2H_5 + C_7H_7^+$. The lines are from modeling, see text. The single point is from measurements of the thermal decomposition of $C_9H_{12}^+$ after conversion through the equilibrium constant.

certainly contribute. Nonetheless, the derived $\langle \Delta E \rangle$ value is not particularly sensitive and was found to be 200 ± 100 cm^{-1}, which, within error, is the same as for $C_8H_{10}^+$ and again similar to the value for neutral propylbenzene.[31]

In order to test the fit, calculations of the thermal dissociation rate were performed using the same expression for $k(E)$ including the J dependence. Without adjusting any parameters, relatively good agreement between the measured, pressure-averaged value at 603 K, *i.e.*, k_{td} = 106 s^{-1} and the predicted value of 46.9 s^{-1} was found, see Fig. 9. This implies that everything is self-consistent and fixes the bond dissociation energy to be E_0 = 166.9 ± 4.2 kJ mol^{-1}.

It is important to point out that the high pressure limiting rate constant for the reverse recombination reaction of C_2H_5 with $C_7H_7^+$, $k_{rec,\infty}(T)$, such as given by,

$$k_{rec,\infty}(T) \approx 8.0 \times 10^{-12} (T/600\ \mathrm{K})^{-1.16}\ \mathrm{cm^3\ molecule^{-1}\ s^{-1}}$$

is much smaller than the Langevin rate constant, $k_L = 1.0 \times 10^{-9}$ cm^3 molecule^{-1} s^{-1}. In other words, $k_{rec,\infty}(T)$ is expected to be much smaller than the Langevin rate constant in the capture of C_2H_5 by $C_7H_7^+$.

Finally, we have extended the temperature range of the instrument even higher (673 K) to study the thermal dissociation of $C_8H_{10}^+$, which occurs at somewhat higher temperatures than does $C_9H_{12}^+$. The results were found to be consistent with the thermal decomposition of $C_9H_{12}^+$, *i.e.* the data indicate that the high pressure limit was observed.[32] A statistical calculation of the complete fall-off curves for both ethylbenzene and propylbenzene cations was also performed[32] so that the data can be used in plasma-enhanced combustion models. A statistical calculation of the complete fall-off curves for both ethylbenzene and propylbenzene cations will be performed so that the data can be used in plasma-enhanced combustion models.

Conclusions

While relatively few studies have been made with the TIFT at AFRL, its value as a new instrument has been proven. The first study of SF_6^- with SO_2 provided no new data but showed that the instrument is capable of accurate measurements over a wide pressure range. This was exploited in studying the reactions of SF_6^- with various solvents where it was found that reaction proceeds in two steps and that the rates are very slow. It is doubtful that as much information could be obtained in any other type of apparatus that is currently available. The large pressure and temperature ranges accessible allowed unique data to be obtained in the charge transfer studies of

O_2^+ with alkylbenzenes. Parent alkylbenzene ions were found to be stabilized at high pressure and to pyrolyze at high temperatures. Combining the data with $k(E)$ measurements and rate theory allowed energy transfer parameters to be measured. It was also found that the magnitude of energy transfer of ions is comparable to that of the neutral counterparts. The analysis also allows bond energies to be derived accurately.

Acknowledgements

This project was funded by the United States Air Force Office of Scientific Research under Project 2303EP4 and Grant Award FA8655-03-1-3034. Financial support of our work by the European Office for Aerospace Research (EOARD grant FA8655-03-1-3034) and by the Deutsche Forschungsgemeinschaft (SFB 357 'Molekulare Mechanismen unimolekularer Prozesse') is gratefully acknowledged.

References

1 W. B. Knighton and E. P. Grimsrud, in *Advances in Gas Phase Ion Chemistry*, ed. N. G. Adams and L. M. Babcock, JAI Press Inc., Greenwich, CT, 1996, pp. 219–258.
2 E. E. Ferguson, F. C. Fehsenfeld and D. L. Albritton, in *Gas Phase Ion Chemistry*, ed. M. T. Bowers, Academic, San Diego, CA, 1979, pp. 45–82.
3 A. A. Viggiano and F. Arnold, in *Atmospheric Electrodynamics*, ed. H. Volland, CRC Press, Boca Raton, FL, 1995, pp. 1–25.
4 S. Williams, A. J. Midey, S. T. Arnold, T. M. Miller, P. M. Bench, R. A. Dressler, Y.-H. Chiu, D. J. Levandier, A. A. Viggiano, R. A. Morris, M. R. Berman, L. Q. Maurice and C. D. Carter, presented at *the AIAA 4th Weakly Ionized Gases Workshop*, Anaheim, CA, 2001.
5 R. A. Morris, P. M. Bench, K. E. Golden and E. A. Sutton, presented at *the 37th AIAA Aerospace Sciences Meeting and Exhibit*, Reno, NV, 1999.
6 J. J. Martin, *Atmospheric Reentry*, Prentice-Hall, Englewood Cliffs, NJ, 1966.
7 J. V. Seeley, J. T. Jayne and M. J. Molina, *Int. J. Chem. Kinet.*, 1993, **25**, 571–594.
8 S. T. Arnold, J. V. Seeley, J. S. Williamson, P. L. Mundis and A. A. Viggiano, *J. Phys. Chem. A*, 2000, **104**, 5511–5516.
9 E. E. Ferguson, F. C. Fehsenfeld and A. L. Schmeltekopf, *Adv. At. Mol. Phys.*, 1969, **5**, 1–56.
10 A. A. Viggiano and S. Williams, in *Advances in Gas Phase Ion Chemistry*, ed. N. G. Adams and L. M. Babcock, Academic Press, New York, 2001, pp. 85–136.
11 A. A. Viggiano and R. A. Morris, *J. Phys. Chem.*, 1996, **100**, 19227–19240.
12 R. L. Daugherty and J. B. Franzini, *Fluid Mechanics with Engineering Applications*, McGraw-Hill, New York, 7th edn., 1977.
13 M. Gilbert, *Combust. Flame*, 1958, **2**, 149–156.
14 F. C. Fehsenfeld, M. Mosesman and E. E. Ferguson, *J. Chem. Phys.*, 1971, **55**, 2115–2120.
15 Y. Ikezoe, S. Matsuoka, M. Takebe and A. A. Viggiano, *Gas Phase Ion-Molecule Reaction Rate Constants Through 1986*, Maruzen Company Ltd, Tokyo, 1987.
16 L. G. Huey, D. R. Hanson and C. J. Howard, *J. Phys. Chem.*, 1995, **99**, 5001–5008.
17 S. T. Arnold and A. A. Viggiano, *J. Phys. Chem. A*, 2001, **105**, 3527–3531.
18 A. I. Fernandez, A. A. Viggiano, T. M. Miller, S. Williams, I. Dotan, J. V. Seeley and J. Troe, *J. Phys. Chem. A*, 2004, **108**, 9652–9659.
19 A. A. Viggiano, T. M. Miller, S. Williams, S. T. Arnold, J. V. Seeley and J. F. Friedman, *J. Phys. Chem. A*, 2002, **106**, 11917–11922.
20 J. Troe, A. A. Viggiano and S. Williams, *J. Phys. Chem. A*, 2004, **108**, 1574–1581.
21 R. A. Dressler and A. A. Viggiano, in *Encyclopedia of Mass Spectrometry-Organic Ions*, ed. M. L. Gross, R. Caprioli and N. Nibbering, Elsevier, Amsterdam, 2005.
22 W. G. Hwang, J. H. Moon, J. C. Choe and M. S. Kim, *J. Phys. Chem. A*, 1998, **102**, 7512–7518.
23 Y. H. Kim, J. C. Choe and M. S. Kim, *J. Phys. Chem. A*, 2001, **105**, 5751–5758.
24 M. Malow, M. Penno and K.-M. Weitzel, *J. Phys. Chem.*, 2003, **107**, 10625–10630.
25 T. D. Fridgen, T. B. McMahon, J. Troe, A. A. Viggiano, A. J. Midey and S. Williams, *J. Phys. Chem. A*, 2004, **108**, 5600–5609.
26 J. Troe, *J. Phys. Chem.*, 1983, **87**, 1800–1804.
27 J. Troe, V. G. Ushakov and A. A. Viggiano, *J. Chem. Phys.*, 2005,submitted.
28 S. Williams, A. J. Midey, S. T. Arnold, R. A. Morris, A. A. Viggiano, Y.-H. Chiu, D. J. Levandier, R. A. Dressler and M. R. Berman, *J. Phys. Chem.*, 2000, **104**, 10336–10346.
29 T. Lenzer, K. Luther, K. Reihs and A. C. Symonds, *J. Chem. Phys.*, 2000, **112**, 4090–4110.
30 E. E. Ferguson, *J. Phys. Chem.*, 1986, **90**, 731–738.
31 H. Hippler, J. Troe and H. J. Wendelken, *J. Chem. Phys.*, 1983, **78**, 6718–6724.
32 A. I. Fernandez, A. A. Viggiano, A. I. Maergoiz, J. Troe and V. G. Ushakov, *Int. J. Mass Spectrom.*, 2005, **241**, 305–313.